DEPARTMENT OF THE INTERIOR

U.S. GEOLOGICAL SURVEY

A High-Resolution Seismic Reflection Investigation of Shallow Horizons at the Denver Federal Center, Lakewood, Colorado

by

Kenneth W. King[1], Robert A. Williams[1] and Robert B. Johnson[2]

Open-File Report 86-448

[1]U.S. Geological Survey
Golden, Colorado

[2]Colorado State University
Ft. Collins, Colorado

CONTENTS

	Page
Abstract	1
Introduction	1
Field site documentation	3
Drill hole data	3
Downhole investigation	6
Refraction seismic survey	9
Reflection field methods	9
Instruments	9
Line geometry--recording parameters	9
Reflection data processing	11
Processing system and sequence	11
Post-stack processing results	15
Data interpretation	18
Seismic modeling	24
Synthetic stack vs. real data	27
Conclusions	27
References	29
Appendices 1 and 2.--Borehole information	30
Appendix 1.--Log of boring 2	31
Appendix 2.--Soil sample test results	34

ILLUSTRATIONS

		Page
Figure 1.	Map showing location of the Denver Federal Center relative to Denver and Golden, Colorado	2
2.	Diagram showing a portion of the seismic reflection line from geophone station 110 to 160	4
3.	Shelby-tube samples	7
4.	Average and interval velocities for a borehole at the Denver Federal Center	8
5.	Reversed seismic refraction profile conducted along the seismic reflection line at the Denver Federal Center	10
6.	Figure (A) shows a cdp gather with the ground-roll outlined. Figure (B) is the amplitude spectrum for part of the trace	12
7.	Figure (A) shows a cdp gather with the ground-coupled air-wave outlined. Figure (B) shows the amplitude spectrum for a portion of one trace	14
8.	Figure (A) shows a cdp gather zero phase band-pass filtered with 3dB down corners. Figure (B) is the same cdp displayed above with nmo correction and mute added	16
9.	Figure (A) is an unstacked cdp with velocity function of figure 3B applied. Figure (B) is a stacked section of 24-fold data. Figure (C) shows the improvement in event resolution	17

ILLUSTRATIONS--Continued

Page

10. Figure (A) is the stacked data of figure 9B with spiking deconvolution applied. Figure (B) is the stacked section of figure 9C with spiking filter applied after the zero phase filter..... 19
11. Figure (A) provides a comparison between spiking and predictive deconvolution. Figure (B) is the data of 11A with a 3-trace mix applied after deconvolution..... 20
12. Reflection data processing sequence..... 21
13. Figure (A) is a re-plot of data from figure 9C. Figure (B) is synthetic stack generated by AIMS..... 22
14. Graph showing depth model used to generate the synthetic stack section..... 25
15. Diagram (A) shows calculated amplitudes and traveltimes generated by AIMS modeling for 12 horizons. Diagram (B) is the result of filtering data of (A)..... 26
16. Figure (A) is the synthetic stack generated by AIMS to compare with real reflection data of (B)..... 28

TABLES

Table 1. Drill hole data..... 5
2. Field parameters and stacking velocities..... 13
3. Interval velocities derived from stacking velocities..... 23

A HIGH-RESOLUTION SEISMIC REFLECTION INVESTIGATION OF SHALLOW HORIZONS AT THE DENVER FEDERAL CENTER, LAKEWOOD, COLORADO

Kenneth W. King, Robert A. Williams and Robert B. Johnson

ABSTRACT

Reflections from several horizons shallower than 50 ft were recorded by seismic reflection methods at the Denver Federal Center in Lakewood, Colorado, by the U.S. Geological Survey in March 1985. Subsurface horizons at depths of 12, 21, 33, and 54 ft produced reflections at 16, 20, 26, and 31 ms, respectively. Refraction, drilling cores, and downhole seismic work provided velocity and depth information that helped identify events on the reflection data. Seismic and drilling investigations allowed construction of a subsurface seismic reflection model. Tests of this model using Geoquest International's Advanced Interpretive Modeling System (AIMS) further substantiated the interpretation of the reflection data.

The seismic reflection work shows successful recovery of subsurface data from depths as shallow as 12 ft with decreasing precision below 30-50 ft for this site. Maximum depths of reliable reflections from subsurface interfaces were 55 ft. The maximum depth drilling was 60 ft. Accuracy of the calculations made from the reflection data are within j1 ft for reflection events at depths of 12 and 20 ft. The accuracy deteriorated to j5 ft for reflection events below a 35-ft depth.

INTRODUCTION

Seismic reflection techniques are increasingly used as a tool in shallow subsurface exploration for targets at depths less than 100 ft (Hunter and others, 1981, 1984). This paper discusses an investigation of shallow reflection methods using a 24-channel digital seismic recording system. The shallow depths of the targets in this study present a new set of field and data processing problems compared to deeper reflection surveys. Interference from large amplitude Rayleigh surface wave trains and the airblast are major obstacles to shallow reflection work. In shallow reflection surveys the Rayleigh and air-blast energy often arrive at the detector simultaneously with the subsurface reflections of interest. Conversely, static corrections and correction for migration often are unnecessary on many shallow reflection surveys because of the reduced scale of exploration.

The objective of this project was to develop procedures for running seismic reflection field surveys and development of data processing techniques to obtain optimum detection of shallow reflections. A four-part comparison program to supplement the reflection work was also undertaken. The location of this work was at the corner of the Denver Federal Center, Lakewood, Colorado (fig. 1). This location was chosen because of its convenience in performing experimental field tests. Each part of the test program involved a different method of measuring and interpretive subsurface properties. The four methods were: seismic refraction, drilling, downhole seismic velocity measurements, and depth modeling using AIMS. The refraction survey was conducted along the same line as the reflection survey. The drilling

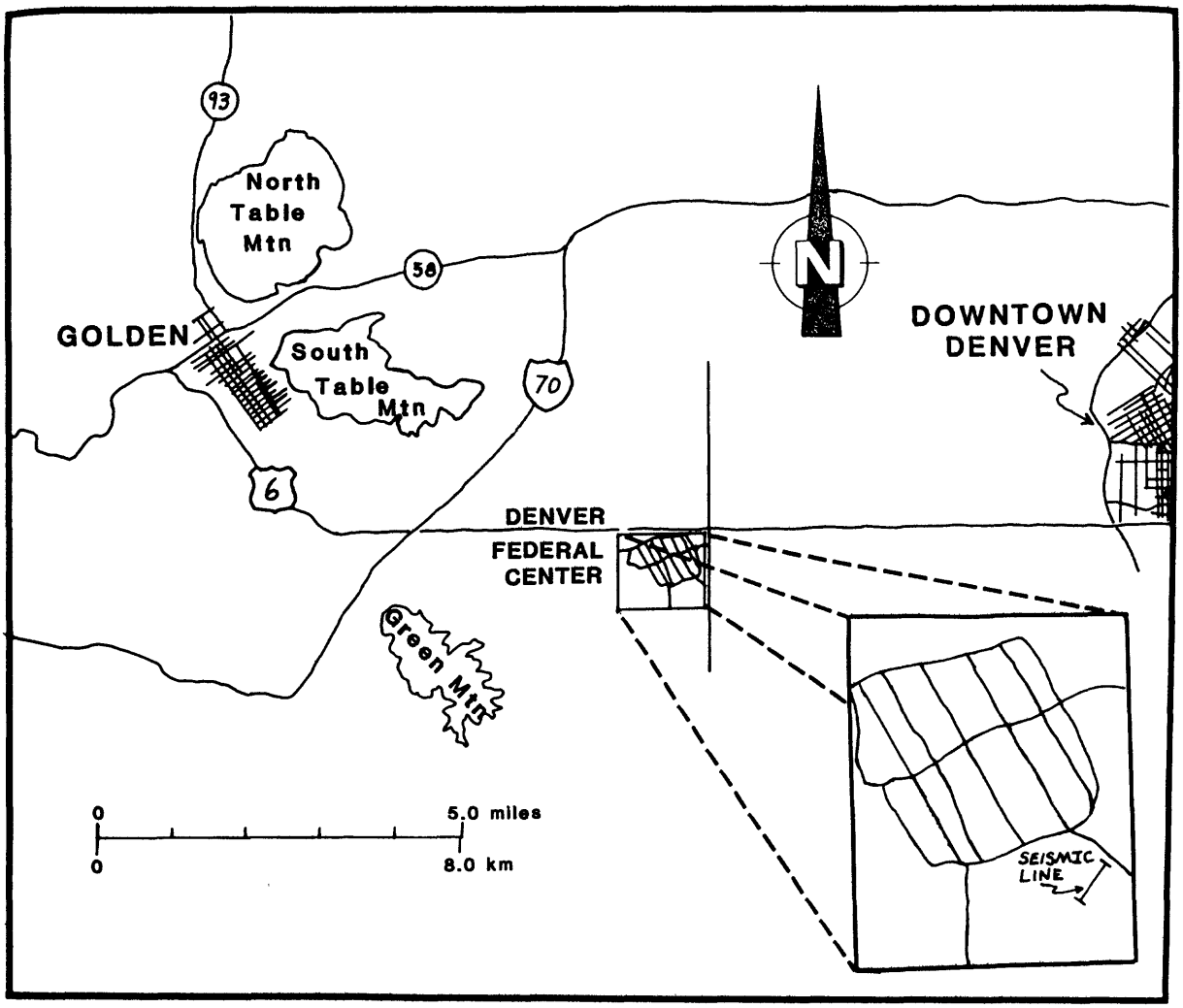

Figure 1.--Map showing location of the Denver Federal Center relative to Denver and Golden, Colo.

consisted of four borings along or near the reflection line (fig. 2): one boring was used for downhole seismic measurements, two others were used to obtain Shelby samples, and the fourth boring was used to provide general information on subsurface geology. The AIMS depth modeling incorporated data from all four parts of the test program.

The first part of this report discusses (a) site geology, (b) drilling procedures and results, (c) refraction data results, and (d) downhole seismic data. The second half discusses (a) reflection field methods, data processing, and results, and, (b) the depth modeling.

FIELD SITE DOCUMENTATION

Subsurface data to document shallow reflections were obtained from a downhole seismic survey and a seismic refraction profile. Documentation focused on determining lateral and vertical changes in materials. All data were obtained along the same line.

Drill Hole Data

Four borings were augered along the reflection alignment as shown in figure 2. Borings 1 and 2 were drilled using a 6-in. outside diameter continuous-flight, solid-stem auger. Borings 3 and 4 were drilled with a 6-in. outside diameter continuous-flight, hollow-stem auger. Hollow-stem augers permitted Shelby-tube samples from intervals selected from downhole seismic profiles and reflection data.

Borings 1 and 2 provided (a) general site information prior to the reflection surveys and (b) cased holes for downhole surveys. Selection of the sites for borings 3 and 4 was based on preliminary interpretation of the processed reflection data.

Borings 1 and 2.--Boring 1 at seismic station 108 on the reflection line (fig. 2) provided general subsurface information from relative changes in augering rate and sample returns at the surface. Water with a static water level of 5 ft was encountered at 13 ft. Sample quality was poor because of mixing with water; the results are not tabulated here. Changes in drilling rate with depth are incomplete due to operation problems and are shown in table 1. Boring 1 was cased with PVC casing which was grouted in place with a 1:1 mix of Portland cement and bentonite.

Boring 2, augered at station 116, again encountered artesian water at 13 ft. Improved sampling was achieved by sampling material from each 5-ft section of auger prior to addition of the next section. The water-bearing zone encountered at 13 ft is perched; most of the deeper materials recovered were dry. The log of relative changes in augering rate (table 1) was more complete than for boring 1. The materials removed from the auger sections were sampled and logged (appendix 1). Grain-size analyses were made as defined by sample study (appendix 2). The sample depth ranges, numbers, and percentage of clay for sample groups are listed in appendix 1. Boring 2 was cased with a 2-in. inside diameter bottom-capped PVC casing and grouted similar to boring 1.

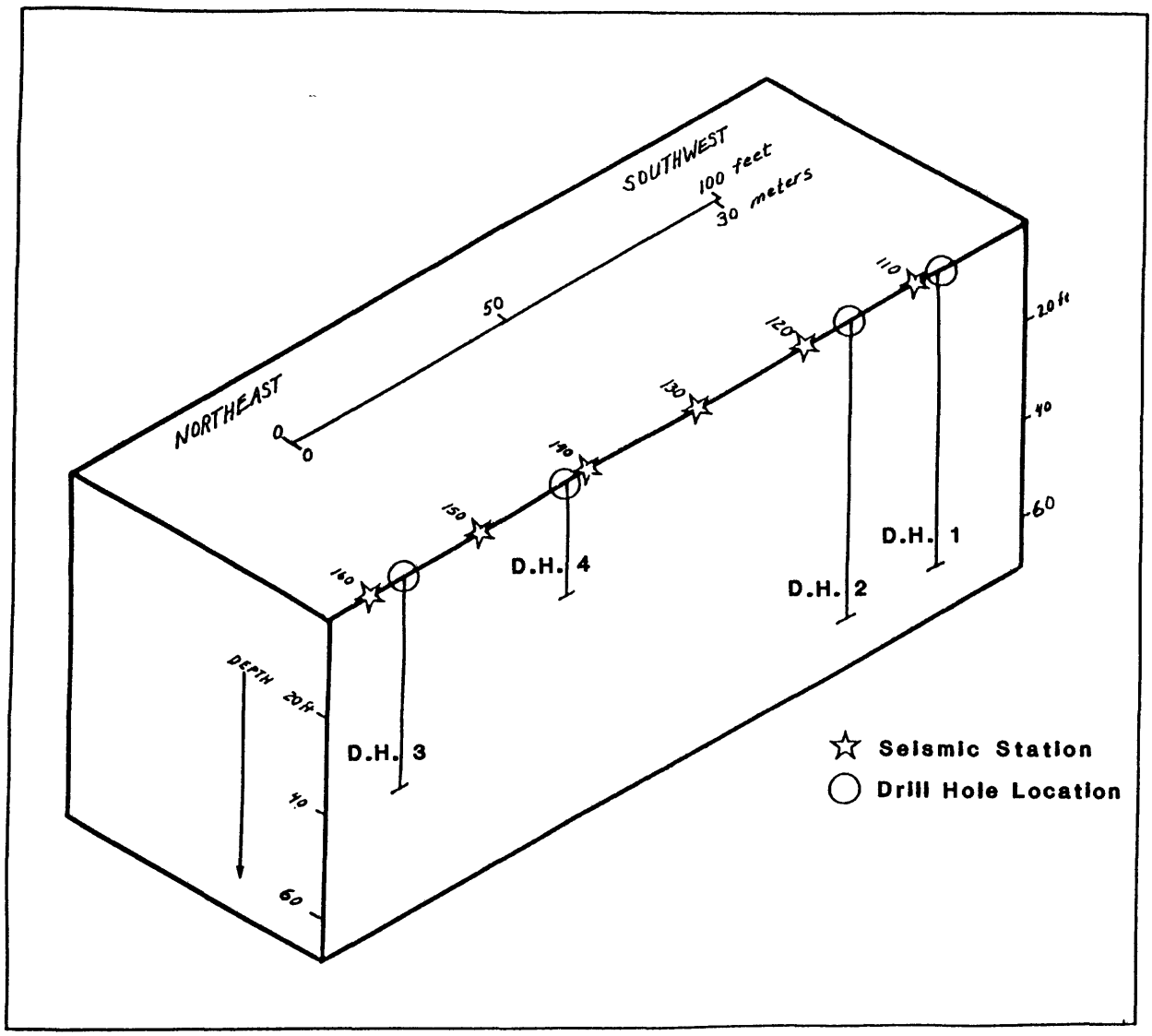

Figure 2.--Diagram showing a portion of the seismic reflection line from geophone station 110 to 160 (every tenth station marked and annotated). Drill hole locations and depths relative to the seismic line are also indicated.

Table 1. - Drill Hole Data

[Sd, loose sand; SS, sandstone; P1, 2, 3, and 4 are photographs shown in figure 3.]

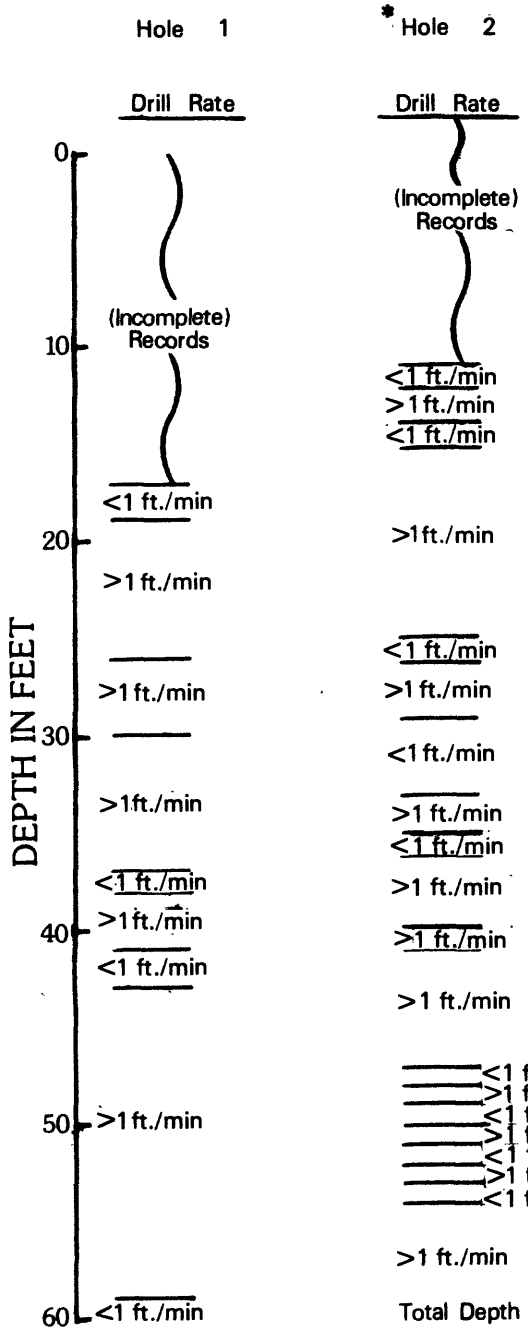

* Hole 2

Drill Rate
(Incomplete) Records
<1 ft./min
>1 ft./min
<1 ft./min
>1 ft./min
<1 ft./min
>1 ft./min
<1 ft./min
>1 ft./min
<1 ft./min
>1 ft./min
<1 ft./min
>1 ft./min
<1 ft./min
>1 ft./min
<1 ft./min
>1 ft./min
<1 ft./min
>1 ft./min
<1 ft./min
>1 ft./min
<1 ft./min
Total Depth

Hole 3

Shelby Tube		Length Drilled (Inches)	Length Recovered (Inches)	Material Log
1		24	22	Sand Clay
2		12	11	
4		16	14	Sd & Gravel
5	P1	30	26	Sd & SS
6		24	28	SS
7	P2	14	16	Clay SS
8	P3	16	16	SS
9		14	11.5	SS & Sd
10		24	15	Clay SS
11		20	24	SS & Sd
12		24	20	Clay
13		18	12.5	Sd
14	P4	18	19	Clay

* Sample locations and descriptions in appendix 1.

Borings 3 and 4.--These borings were drilled with hollow-stem augers; samples were taken by Shelby-tubes. Confined water was at the same depth and under similar head conditions as in borings 1 and 2.

Boring 3 was located at seismic station 157 where preliminary analysis of the shallow reflection events indicated horizontal, continuous reflecting surfaces. Shelby-tube samples were obtained for depth zones chosen from a combination of downhole velocity information from boring 1 and reflection events. The samples contained the same gravel-size pieces of angular siltstone and sandstone found in boring 2. They are from moderately- to well-lithified sandstones having differing amounts of silt- and clay-sized material. Sample depths, lengths, recovery, and materials are given in table 1. Detailed logs of Shelby-tube samples are in appendix 1.

The correlation of recovered materials from boring 3 and the downhole seismic velocities (next section) obtained from the boring, 130 ft distant, provides the basis for the conclusions presented in this open-file report. Photographs of selected Shelby-tube samples from boring 3 illustrate the lithified character of the higher velocity materials (fig. 3a,3b). We assume that these cemented zones are correlated with those in boring 1. Figure 3c, and 3d portray selected lower velocity intervening materials. These materials may be compared with the zones of rapid and slow drilling encountered in boring 2. It should be remembered that auger rates in uncemented gravels can mimic rates in lithified sand and silt. Locations of photographs of Shelby-tube samples are noted by "P" on table 1.

Drill hole no. 4 is located at station 142 where reflection data indicate a shallow depression in a reflector at approximately 20 ft. Shelby-tube samples from the zone (18.5-22.5 ft) did not find a depression in this reflecting horizon.

Downhole Investigation

A downhole survey was run in hole no. 1 to document velocity changes occurring at depth for use in evaluating reflection data. A Mark Products Model L-10, 8-Hz downhole geophone assembly was used to record arrival times from a hammer source located on the surface 5 ft from the casing wall. A Bison Model 1416 signal enhancement seismograph was used for determining signal arrival times. Starting at the surface, arrival times were recorded at 2-ft intervals to the bottom of the hole at 60 ft.

Downhole and interval velocities for boring 1 are shown in figure 4. Comparison of depths of significant velocity changes with changes in sample material from boring 3 imply lateral continuity of subsurface units between borings 1 and 3. With the exception of an anomalous reflector at about 20 ft at boring 4, reflection data show similar lateral continuity. The samples from boring 4 at 20 ft are visually identical to samples from 20 ft at boring 3. The samples are consistent with high-velocity material occurring at 20 ft shown by the downhole survey.

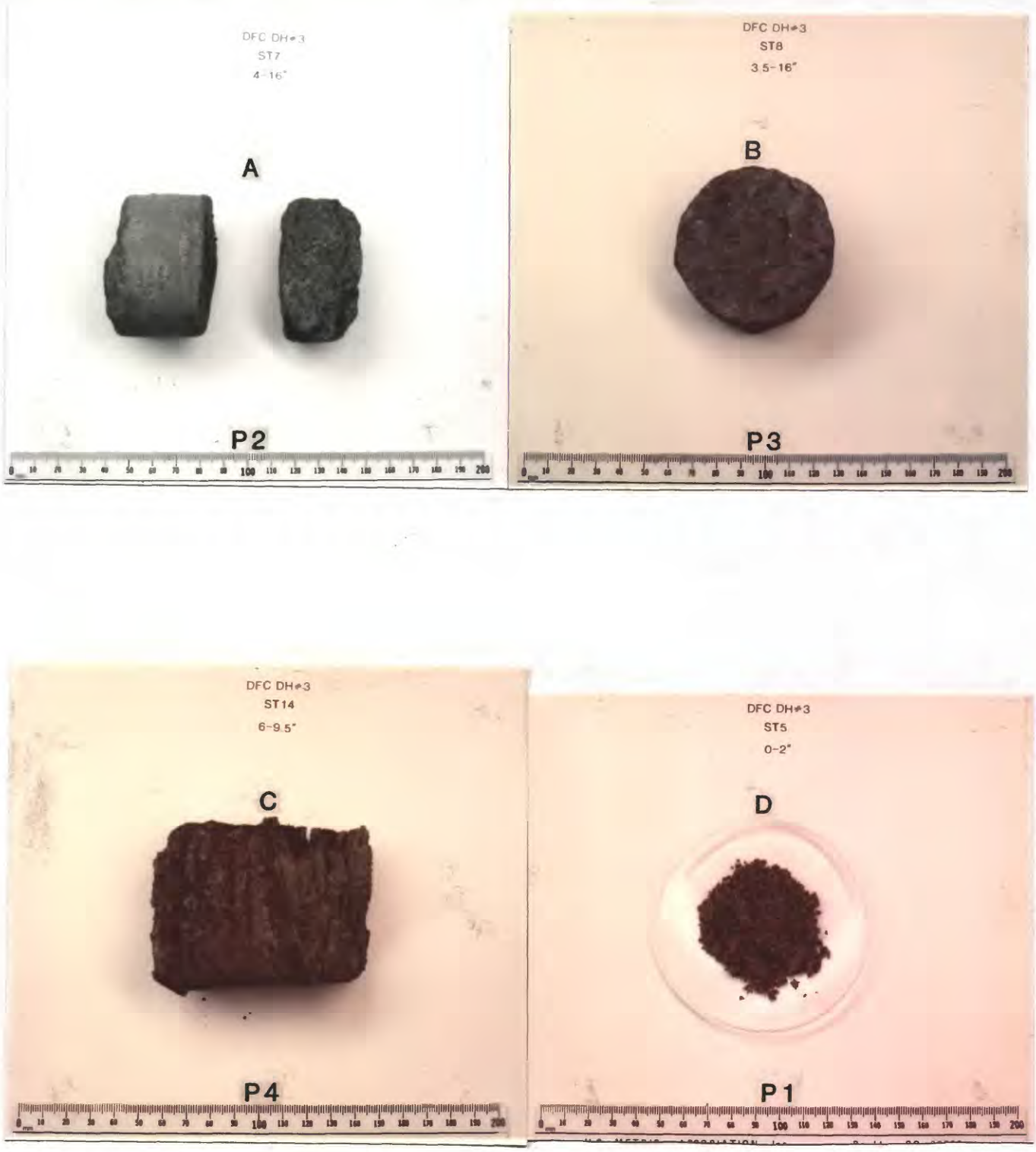

Figure 3.--Shelby tube samples from boring 3. Samples A and B are more well cemented than samples C and D. The locations of samples from boring 3, photographed above, are designated P1, P2, P3, and P4 in table 1.

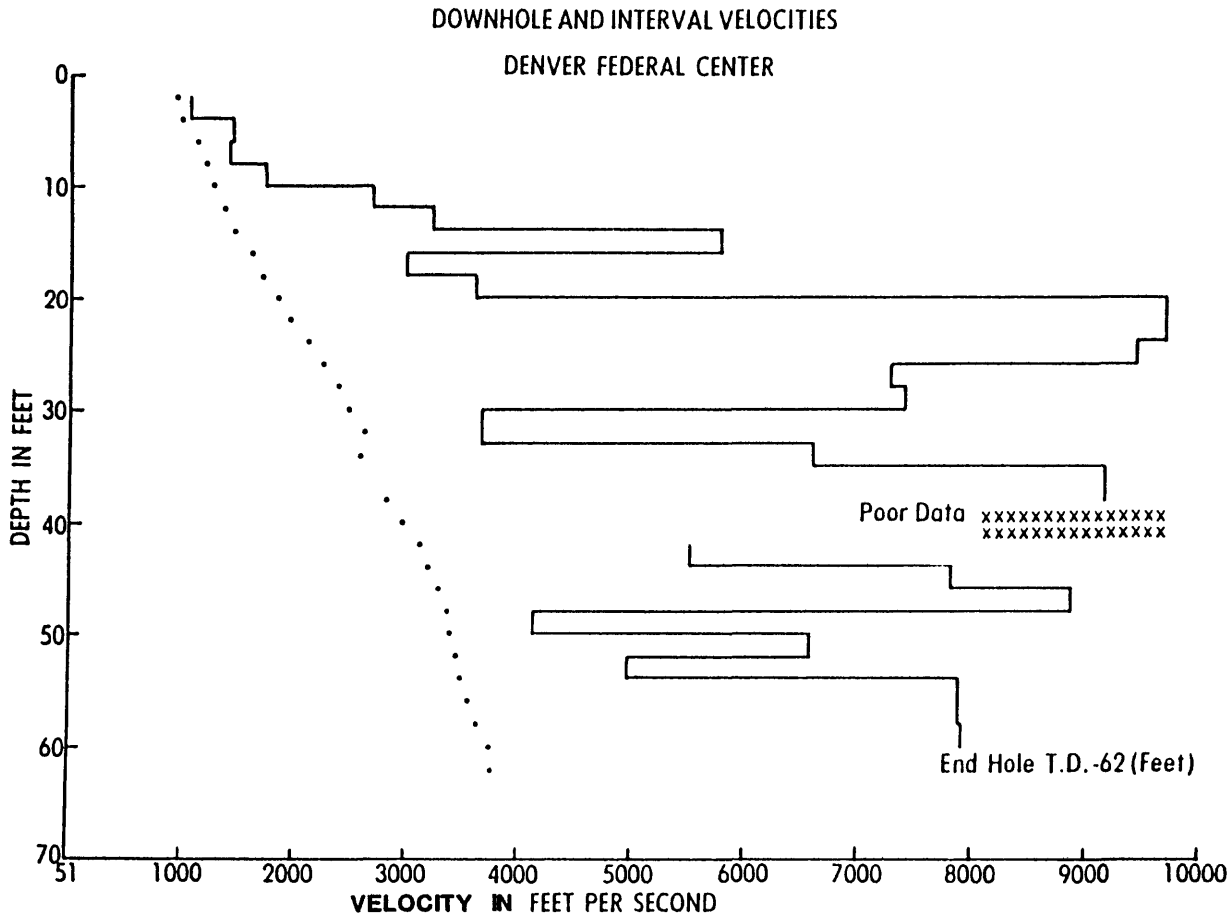

Figure 4.--Average (dots) and interval (solid lines) velocities for a borehole at the Denver Federal Center, Lakewood, Colo. The borehole is located 10 ft from the seismic reflection profile.

Refraction Seismic Survey

The Denver Federal Center site was surveyed by use of the reversed-profile refraction seismic technique. Data from a 6-channel Bison Model 1580 signal enhancement seismograph and a single-channel Nimbus ES-125 signal enhancement seismograph combination was used to construct a traveltime graph shown in figure 5. Energy sources consisted of a 12-gauge shotgun (Betsy Seisgun) for the Bison unit and an 8-lb hammer for the Nimbus unit. The reversed profile extended along the reflection line from station 108 and hole no. 1 to station 148.

Record samples and augering rates from borings 1 and 2 indicate that alternating high- and low-velocity beds would preclude seismic signals from all material contacts. Thus, we did not expect to accurately calculate depths to all the beds identified with downhole and reflection methods. Both the velocities and calculated depths to the first velocity interface in figure 5 correspond well with the data from the downhole seismic survey (fig. 4). The higher velocities and calculated depth from a third refracting interface appear to correlate with the 9700-ft/s layer encountered in the downhole survey. The scatter of the first arrivals of the refraction seismic signals from the apparent second layer are due to the presence of alternating thin beds of high- and low-velocity material (fig. 5). This interpretation is supported by the downhole seismic survey.

REFLECTION FIELD METHODS

Instruments

An Input-Output Inc. DHR-2400 24-channel seismic recording system was used to collect the reflection data. Amplifiers on the DHR-2400 controlled the relative signal input level of all 24 channels individually. The system produces demultiplexed common-source-point "gathers" and writes them to digital tape in fixed-point 32-bit words (Input-Output, Inc., 1980). Single 100-Hz geophones with 6-in. planting spikes were used for each recording station. A 12-gauge Betsy Seisgun that vertically fires a 1-oz lead slug provided the energy source for this experiment.

Line Geometry--Recording Parameters

A linear geophone array of 24 individual geophones planted 5 ft apart with 12 to each side of the source was used for this experiment. The geophone nearest to the source was 10 ft away and the farthest was 65 ft away. The geophone array and source was moved linearly from southwest to northeast at 5-ft intervals for each shot. The seismic line was a split-spread which rolled on, across, and off the geophone array at 5-ft intervals (Lang, 1980) (fig. 1). The geophones were planted, on an average, 4 in. below the surface to improve the geophone-earth coupling. Source coupling was also enhanced by augering the shotholes 4 in. below the sod into which the shots were fired. The material at the geophone and shotpoint base locations was a more dense clay-rich layer (1200 ft/s) than the aerated loosely consolidated soil on the surface (600-800 ft/s). Two shots were fired at each station. The second shot improved the recorded signal by increasing the signal to noise ratio and

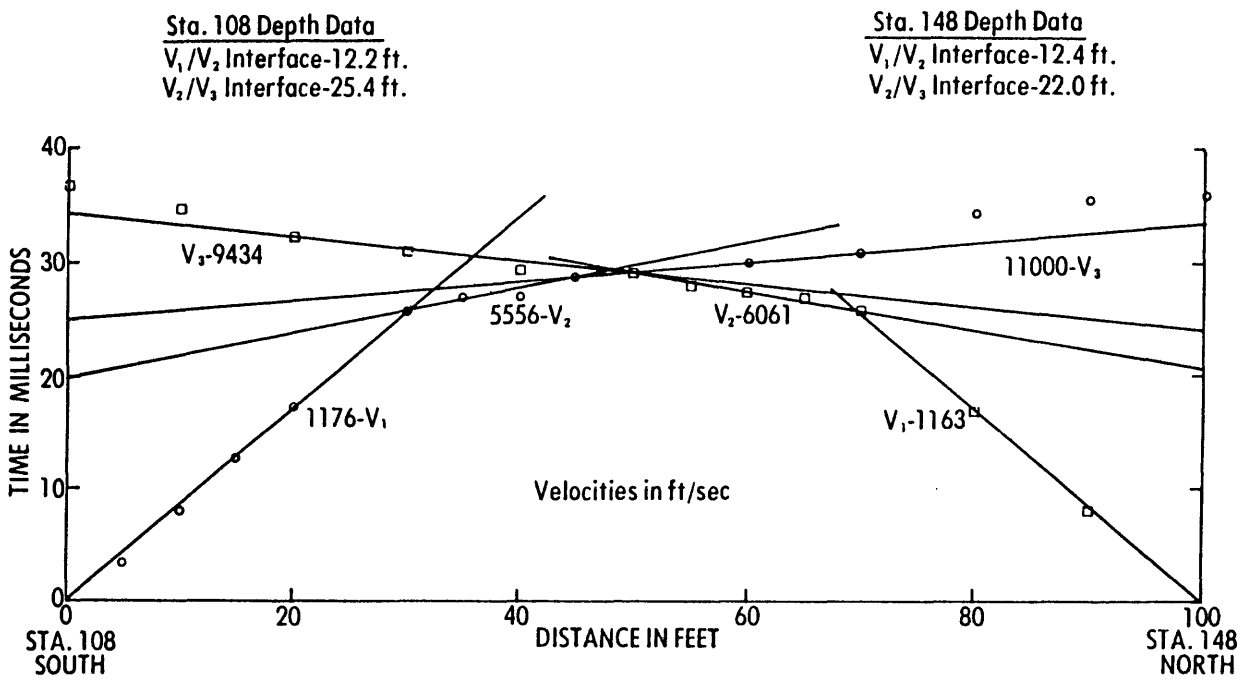

Figure 5.--Reversed seismic refraction profile conducted along the seismic reflection line at the Denver Federal Center, Lakewood, Colorado.

by increasing the overall signal strength. Firing a third shot into the same hole did not significantly improve data quality. Slug penetration averaged about 1 ft for this site. Summation of common-source-point files occurred during the processing phase. Shooting the line twice produced 24-fold common-depth-point (cdp) data in the following manner: after one pass of the source along the full length of the line with the above configuration, the source was brought back to the beginning and the entire line was shot again in the same fashion except that all geophone positions were advanced one-half station interval (2.5 ft). A sample period of 0.25 ms with 1000 samples per trace produced 250-ms records. An 80-Hz (3 dB down at 80 Hz at 24 dB/octave) high-pass field recording filter was used to try to reduce ground-roll (Rayleigh waves) energy which peaked at 60 Hz for this site (figs. 6a, 6b). An attempt to shield geophones from an expected large amplitude air wave was made by planting the phones in shallow holes; the geophones were also shielded by placing a small sandbag over the hole. Although the air-wave energy was reduced the air-wave energy still displays substantial energy on our records. We suspect that the air-wave is ground-coupled as suggested by Mooney and Kaasa (1962). Table 2 contains a summary of the recording parameters used in this study.

REFLECTION DATA PROCESSING

Processing System and Sequence

The 24-fold field data were processed at the U.S. Geological Survey's seismic data center at Denver Federal Center, Lakewood, Colorado. The processing software consists of Digicon's DISCO system installed on a Digital VAX 11/780 computer.

Initially the field data had to be converted from its modified SEG-Y form to the DISCO format in order to process the data on the VAX. Plotting of raw field records allowed examination of individual records to note any poorly recorded traces and to inspect the overall quality of signal-to-noise ratios. Traces judged to be poor in quality were removed from further processing. The strong ground-roll and ground-coupled air-wave dominating the early part of the record were also observed at this stage (fig. 7a). All reflection data were scaled with 40 ms agc before plotting. These high-energy signals present in the shallow section required low-gain settings in order to record them without saturating the amplifier. The low-gain settings precluded the possibility of recording low-energy reflection data later in the record. Therefore, only the first 50 ms were judged to contain valid reflection data; the last 150 ms duration of the recorded data were eliminated from further consideration. The high-pass field filter designed to attenuate ground-roll and air-wave energy was not as effective as we had hoped, primarily because measurements of raw field traces showed that the air-wave energy peaked at 100 Hz (fig. 7B), which was 20 Hz above the cutoff of the recording filter. One unexpected signal conditioning advantage found on this experiment was the strong attenuation of refraction energy due to geophone frequency and field filter settings. The frequency of refraction energy is below 50 Hz and does not interfere with the reflected energy. Therefore, no special processing procedures were necessary to eliminate it.

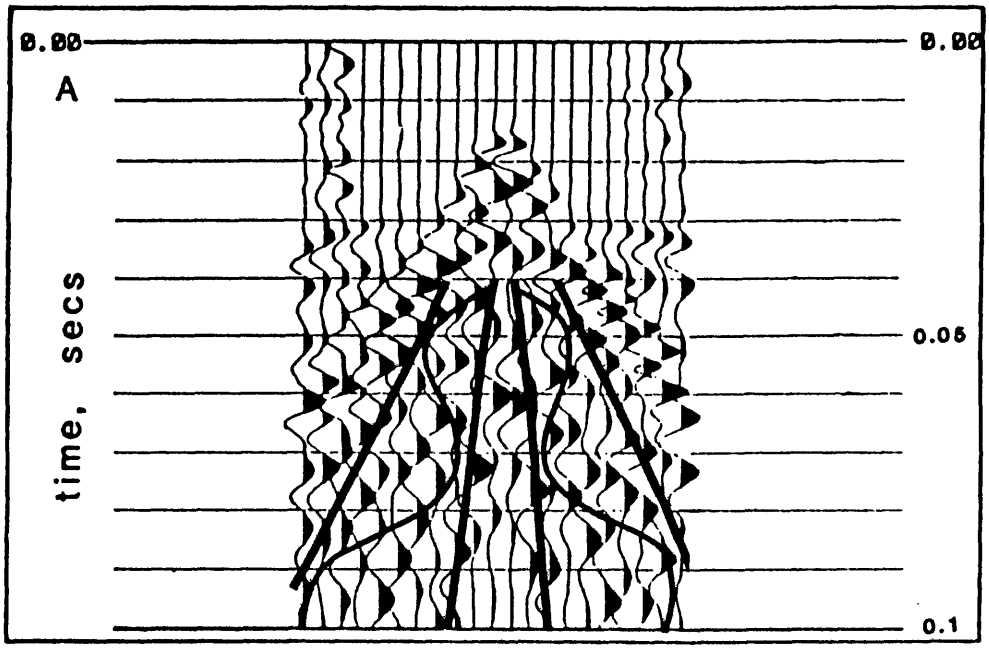

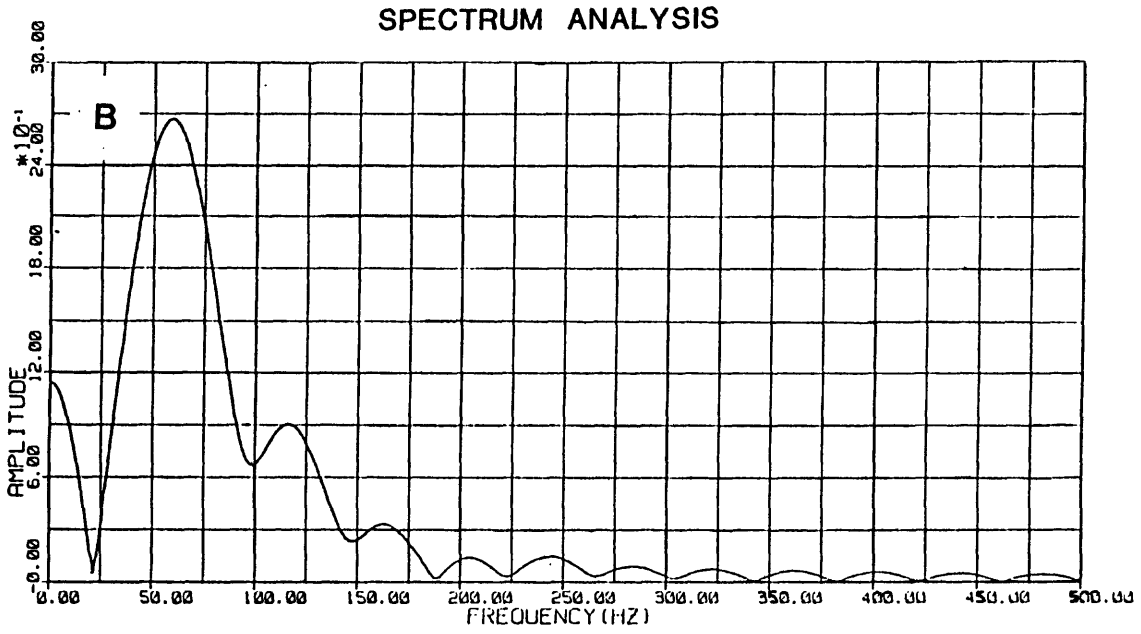

Figure 6.--Top figure (A) shows a cdp gather with the ground-roll outlined. No nmo (normal moveout) correction, filter, or mute has been applied to this data. Bottom figure (B) is the amplitude spectrum for the part of the trace, from the cdp gather above, which contains primarily ground-roll energy. The spectrum shows that the frequency of this energy peaks at approximately 60 Hz.

Table 2.--Seismic reflection field parameters

Field parameters	
Type instrument---DHR-2400	Energy source------12-gauge shotgun
Tape format-------Modified SEG-y	Type projectile----1-oz hollow point slug
No. channels------24	Shots/shotpoint----2 shots/SP
Field filter------80 Hz high-pass 24 dB/octave	SP interval--------5 ft
Fold--------------24	Geophone interval--5 ft
Geophone array----Single 100 Hz	Field geometry-----65-10 x 10-65 ft

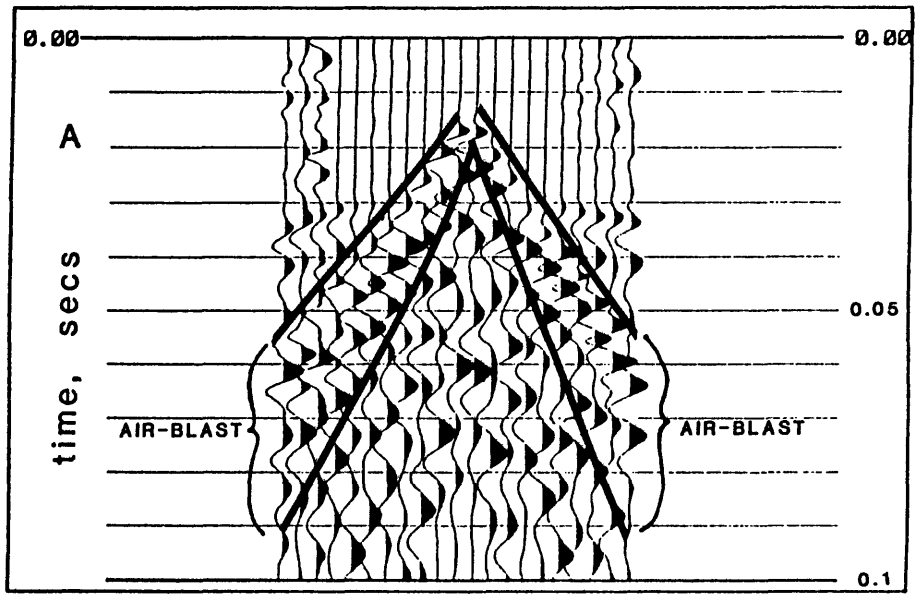

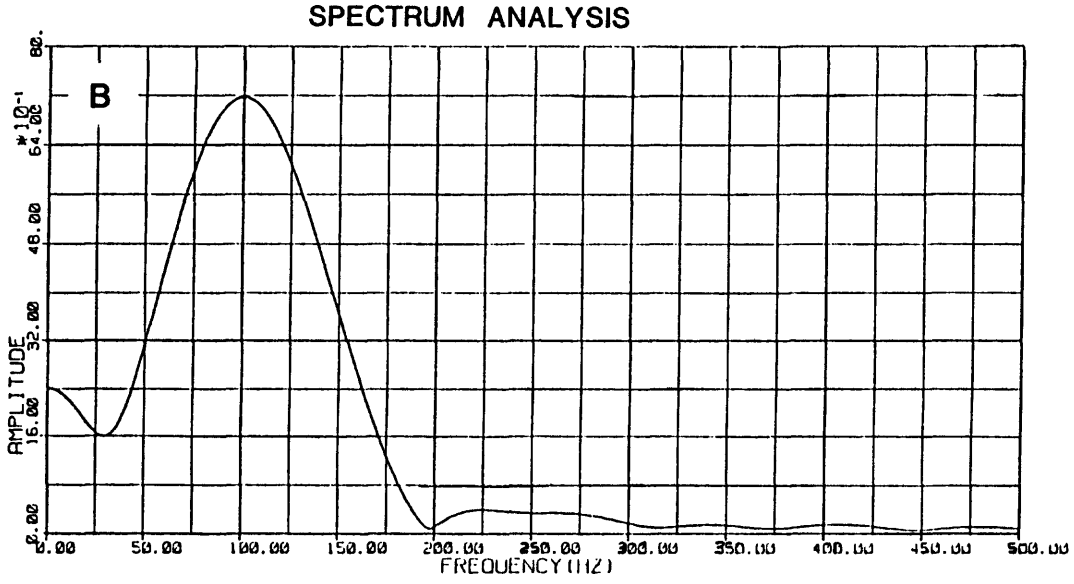

Figure 7.--Top figure (A) shows a cdp gather with the ground-coupled air wave outlined. No filter, nmo correction, or mute has been applied. Bottom figure (B) shows the amplitude spectrum for a portion of one trace (from the above cdp gather) which is dominated by air wave energy. The spectrum shows that the dominant frequency of the air wave is approximately 100 Hz.

Based on the above filter tests, a filter was designed to help reduce ground-roll and air-wave energy. Figure 8A shows how a zero-phase band-pass filter, 3 dB down at 150 and 400 Hz (the pass band) and falling off 18 dB/octave outside this band, helps attenuate lower frequencies.

The pair of shots recorded at each shotpoint were summed into one common file during the processing phase rather than summed in the recording system to better observe the effectiveness of reflection energy enhancement by vertical stacking on the higher resolution plotter in the processing center. The summing procedure showed a slight increase in reflection energy on the event observed at 30 ms while ground-roll and air-wave energy remained constant. A technique called muting eliminates unwanted information from the seismic reflection data by forcing the recorded amplitude values to a value of zero within any designated time zone. Muting was used on this data to help reduce the influence of ground-roll and air-wave energy.

Figure 8B shows a cdp gather with the mute applied. Use of an f-k (frequency-wavenumber) velocity filter did not prove effective in attenuating this energy. Muting followed normal-moveout (nmo) correction in the processing sequence. A flat line profile eliminated the necessity of performing elevation corrections. Additionally, corrections for velocity variance due to weathering were unnecessary as reflection events on the stack records proved to be relatively flat. The near-surface low-velocity layer is parallel to underlying bedding and has uniform velocity and thickness along the length of the array line and, thus, does not create a surface velocity problem.

For purposes of velocity analysis, the data were collected into cdp summed records or "gathers" with a maximum of 24 traces in each "gather." With the aid of downhole and refraction data, velocity picks were made from a group of constant velocity trials. The downhole and refraction data provided a framework for velocity possibilities and improved confidence in selection of velocities. Table 2B shows the velocity function used on this data set to correct for nmo. Figure 9A shows at least one event in the unstacked gathers responding to the nmo correction velocity by changing from a curving reflector that spans a time from 31 to 33 ms to a flat event at 30-31 ms.

Post-Stack Processing and Results

Once the pre-stack spectral, mute, and velocity analyses were completed the data were stacked. Figure 9B shows a stacked section with 24-fold traces. The fold actually fluctuates between 24 at 20 ms, dropping off where the mute becomes more severe, and then building back up again to 24 at about 75 ms. Events before 30 ms are twofold to eightfold depending on the time of the event.

Post-stack spectral analysis revealed the reflection events to have spectral peaks between 200 and 250 Hz. Therefore, a post-stack filter, designed to enhance this energy, consisted of a 200-250 Hz pass band and 3 dB corners at 200 and 250 Hz. The falloff in energy outside the pass band occurs at a rate of 18 dB/octave. Figure 9C (with the post-stack filter) can be compared to figure 9B (without the post-stack filter). An event at 27 ms becomes more prominent with use of this filter post-stack; however, the filter

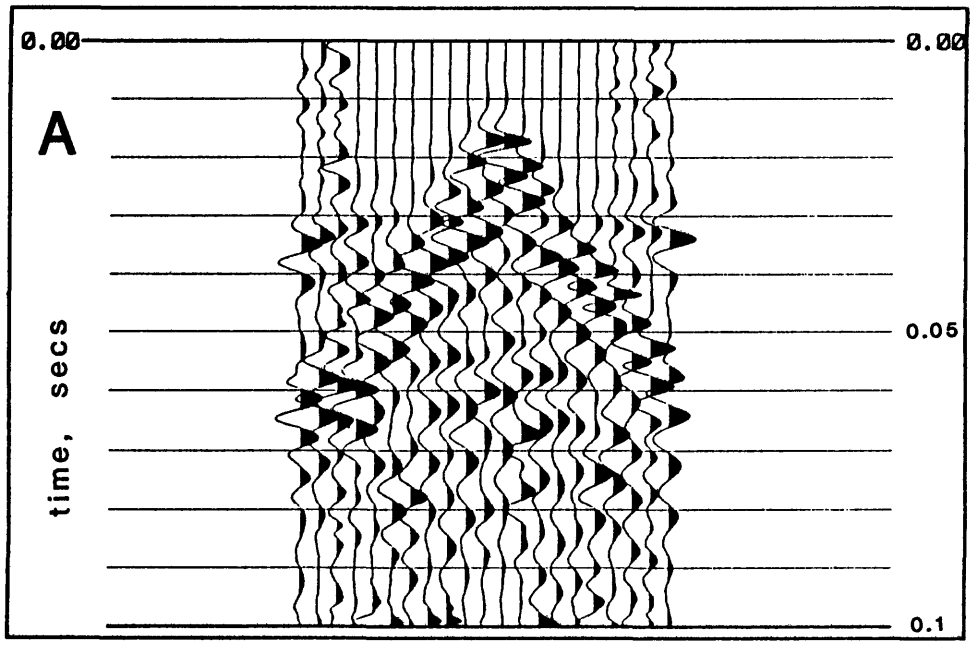

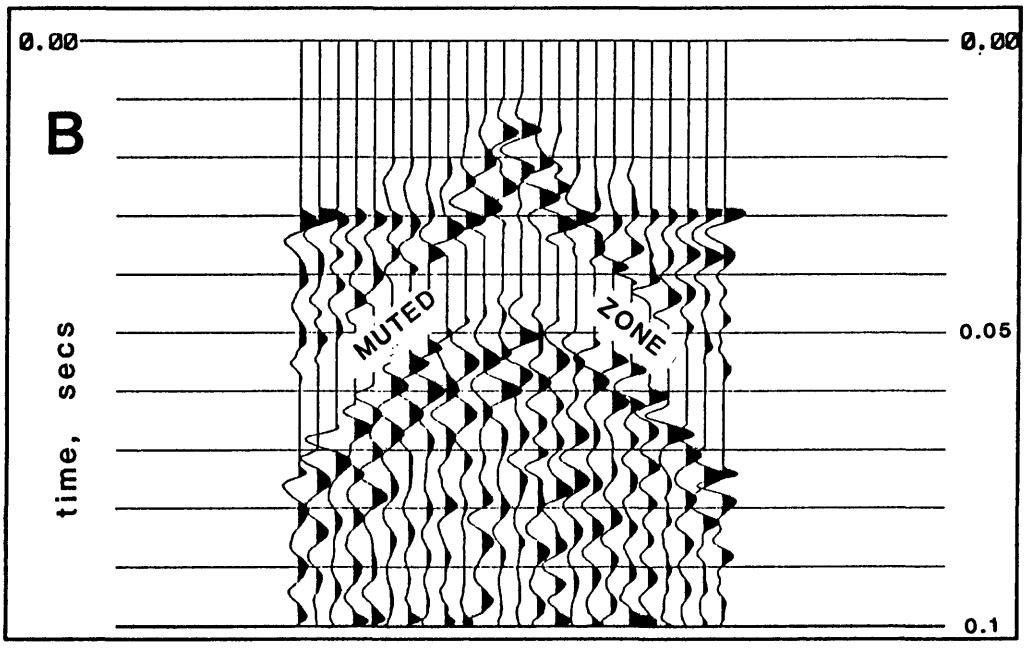

Figure 8.--Top figure (A) shows a cdp gather zero-phase band-pass filtered with 3 dB down corners at 150 and 400 Hz and 18 dB/octave attenuation outside this band. No nmo correction or mute has been applied. Ground-roll energy is strongly attenuated by this filter while the air blast remains quite strong. Bottom figure (B) is the same cdp displayed above but with nmo correction and mute added. Muting was performed to reduce the influence of the air blast.

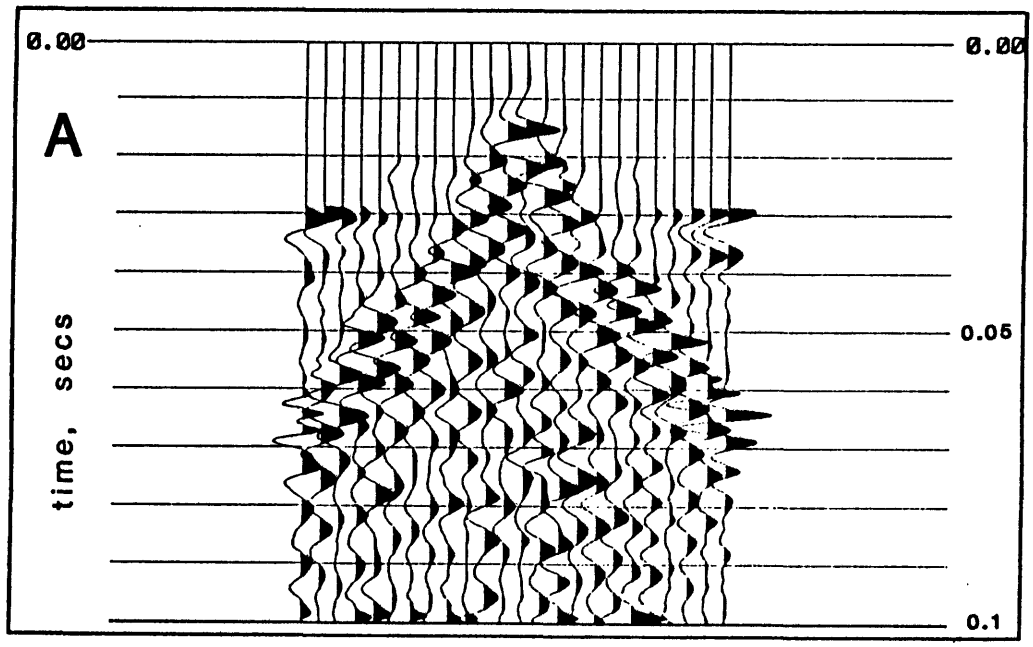

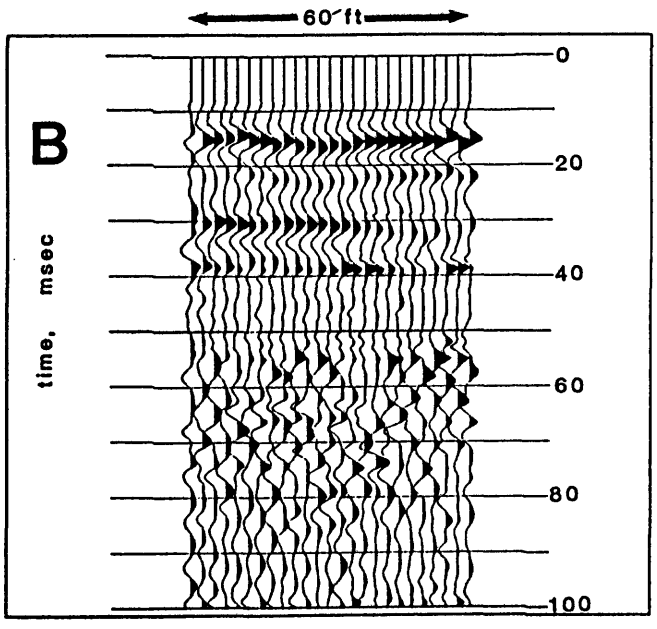

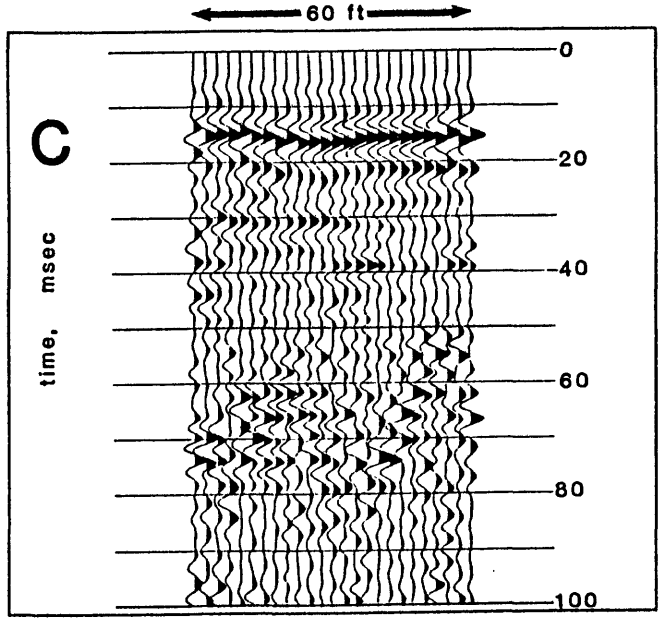

Figure 9.--Top figure (A) is an unstacked cdp with the velocity function of figure 3B applied. Reflection event at 30 ms has been flattened by application of this velocity function. Figure at bottom left (B) is a stacked section of 24-fold data. Bottom right figure (C) shows the improvement in event resolution, as compared to 9B, after application of a post-stack filter.

that follows the stacking process has some side effects. The events prior to 14 ms are actually artifacts of the filtering process. The convolution of the filter with low energy noise prior to any reflection data generates a false coherent event.

Tests of deconvolution applied to pre-stack versus post-stack data show that deconvolution performs better when applied post-stack. Resolution is higher and undesirable noise generating effects of the deconvolution are reduced. Stacking the data achieves better signal to noise ratio (through noise cancellation) and allows for a more effective and realistic deconvolution. Many authors (Berkhout, 1977, Sengbush, 1983, Jurkevics and Wiggins, 1984) have written of the need for a high signal to noise ratio in order to achieve accurate deconvolution results. The stacking process here helped build signal and cancel random noise events. Berkhout (1977) also mentions the practice and possible need of zero-phase filtering before deconvolution in cases of low signal and high noise despite theoretical considerations which assume a minimum-phase input to the deconvolution process. Tests of zero-phase filtering before deconvolution showed that it was a desirable procedure for this data set as well (fig. 10). Results of spiking versus predictive deconvolution showed spiking to be preferable in several categories; a broader bandwidth, smoother amplitude spectrum and higher resolution were attained with spiking deconvolution (fig. 11A). One disadvantage of spiking deconvolution compared to predictive deconvolution in this case is that greater time shifts occur using the spiking filter. Analysis of autocorrelations on these data showed that multiple energy was not a problem. Deconvolution was used here solely as a means to increase high-frequency energy, broaden and balance the spectrum, and contract the seismic pulse. As applied to this data, the deconvolution process did achieve these goals.

Results of a trace mixing program applied to stacked data are shown in figure 11B. Trace mixing improves event coherency by decreasing the heterogeneity of trace to trace differences. It can help enhance general patterns or relationships within a stacked section. The trace mix used on this data set produced one output trace that replaced the middle trace of every trio of input traces summed. The process then moves ahead one trace and repeats until reaching the last trace specified by the processor. Figure 12 summarizes the processing sequence used on this data set.

DATA INTERPRETATION

The stack section (without deconvolution) of figure 13A reveals four coherent events that can be correlated to acoustic boundaries interpreted from drill core samples (Shelby tubes), downhole and refraction data. The events occur in time on the reflection record at 16, 20, 26, and 31 ms. The Dix formula can be used to calculate interval velocities (V_i) from stacking velocities of table 3 as follows:

$$V_i = \left[\frac{V_2^2\, T_2 - V_1^2\, T_1}{T_2 - T_1}\right]^{\frac{1}{2}}$$

where V_2 and V_1 are the root-mean-square (rms) velocities to two reflections with respective times of T_2 and T_1, and V_i is the interval velocity between

ZERO PHASE FILTER EFFECTS WHEN APPLIED BEFORE DECONVOLUTION

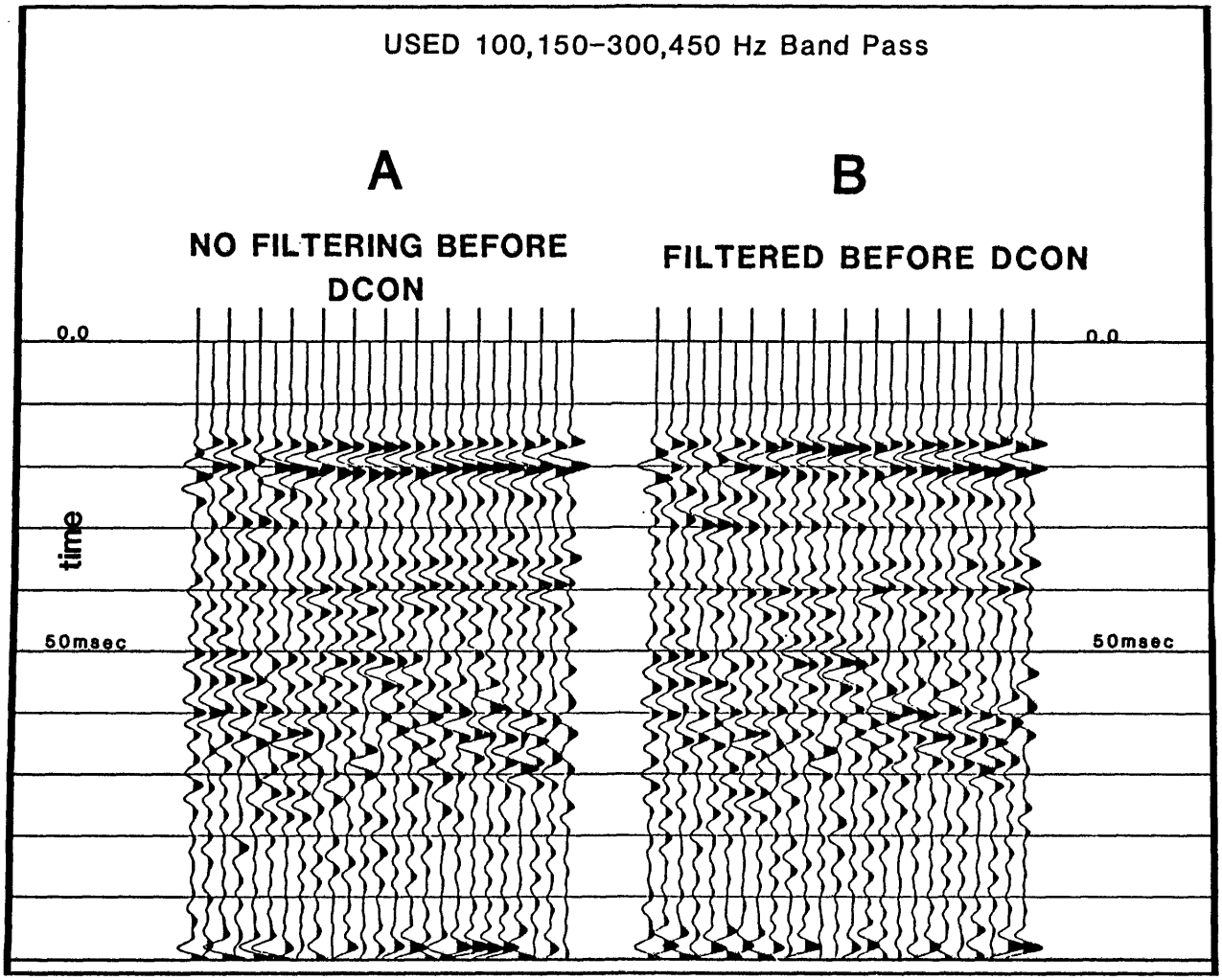

Figure 10.--The figure on the left (A) is the stacked data of figure 9B with spiking deconvolution applied - no filtering was done prior to deconvolution. The figure on the right (B) is the same stacked section of 9C but with the spiking filter applied after the zero-phase filter. Applying deconvolution after the zero-phase filter improves event resolution between 20 and 30 ms. The parameters for deconvolution on A and B above are identical. The coherent events seen below 35 ms are not considered valid.

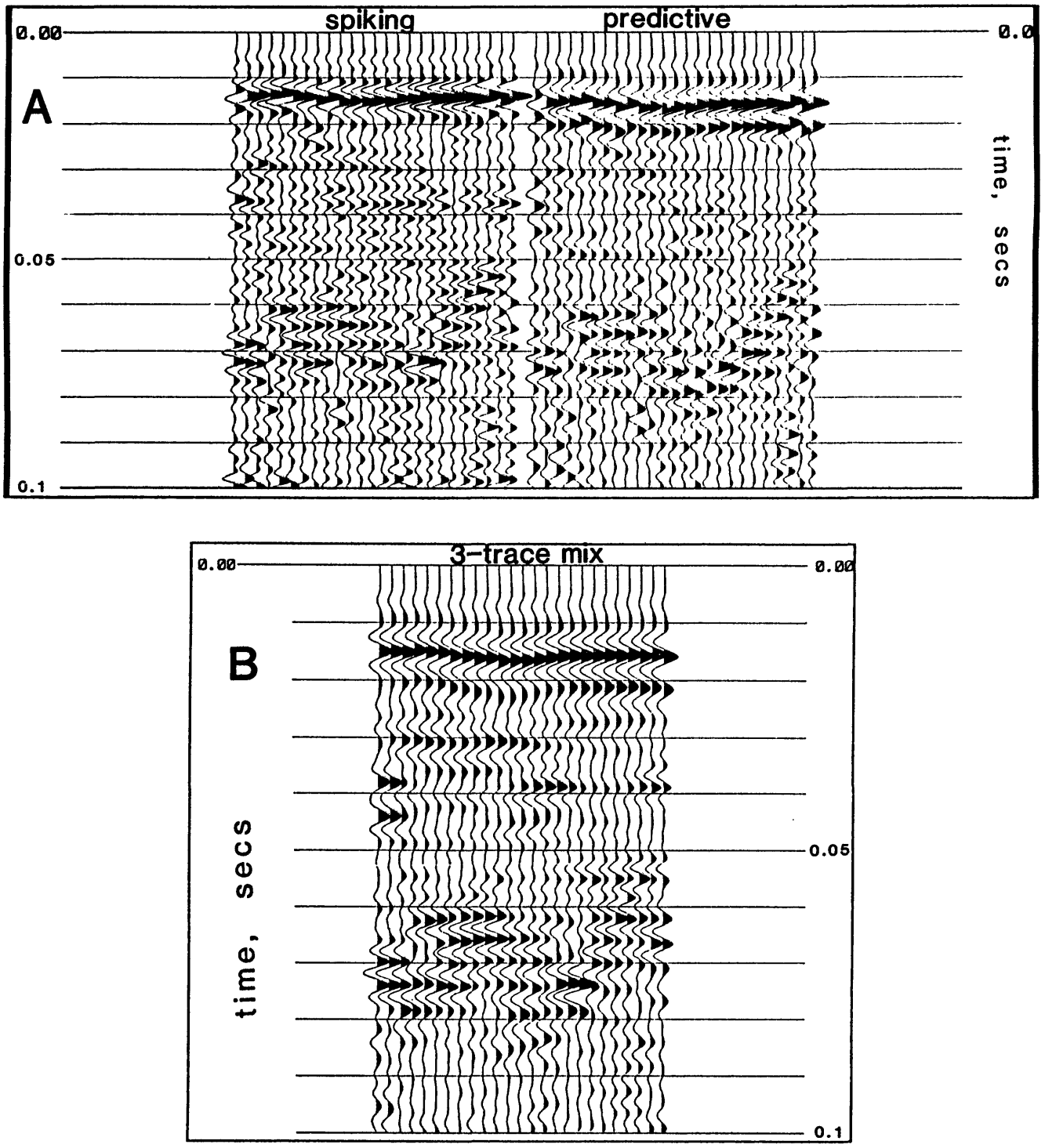

Figure 11.--The top figure (A) provides a comparison between spiking (on the left) and predictive (on the right) deconvolution. Again, event resolution between 20 and 30 msec is better for spiking than for predictive deconvolution. The predictive deconvolution parameters are: prediction distance equals the 2nd zero crossing with a 40 msec operator length. The spiking deconvolution parameters are the same as in figure 10B. The bottom figure (B) is the data of 11A (left side) with a 3-trace mix applied after deconvolution. All deconvolution filters were applied after stacking.

1. Reformat field data from modified SEG-Y to DISCO format.

2. Trace edit.

3. Vertical stack.

4. Geometry definition.

5. cdp sort.

6. Filter analysis.

7. Velocity analysis.

8. Mute analysis.

9. Brute stack.

10. Re-analyze velocities, filters, and mutes.

11. Stack.

12. Deconvolution.

13. Trace mixing.

14. AGC (Automatic Gain Control Scaling)

Figure 12.--Reflection data processing sequence.

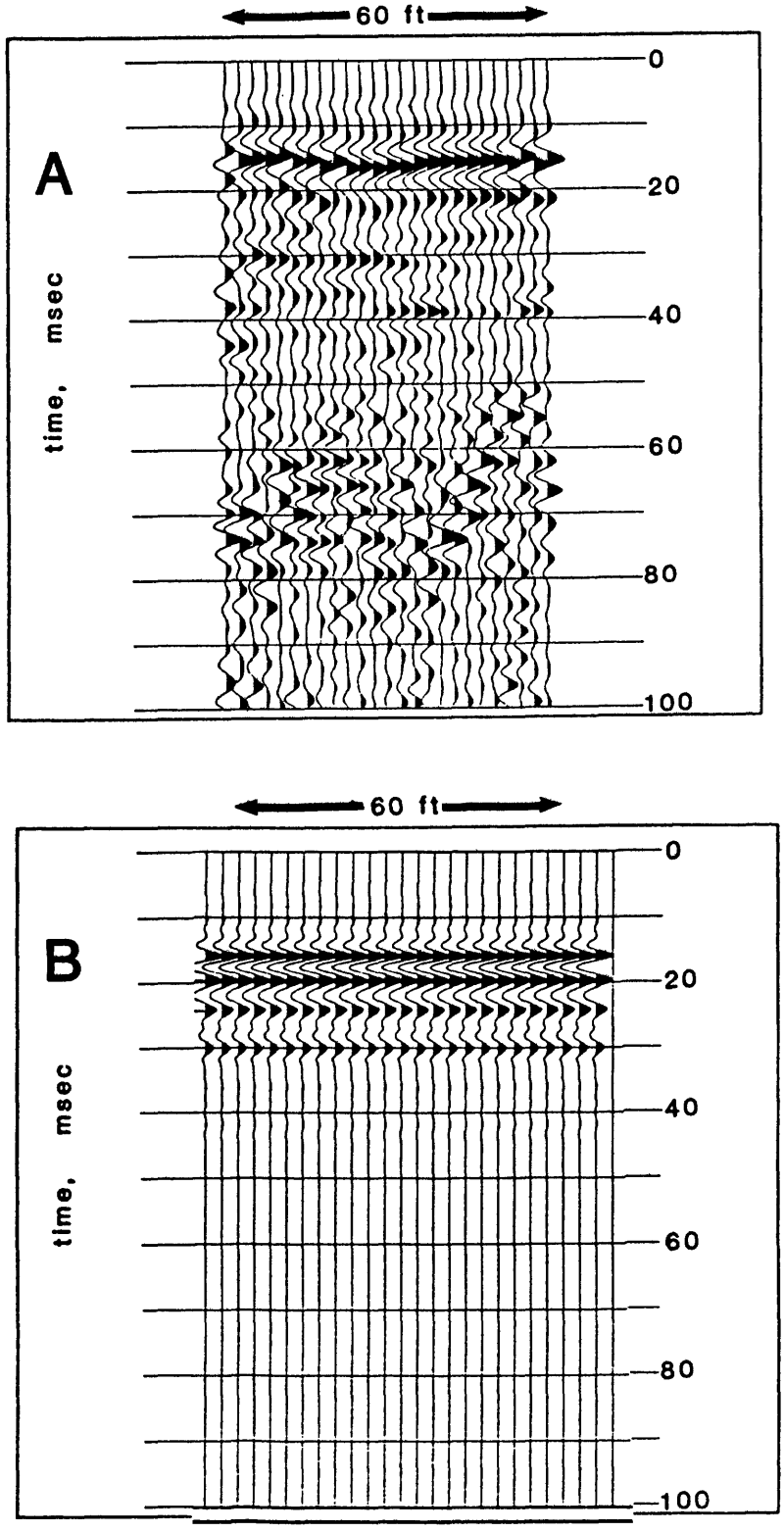

Figure 13.--The top figure (A) is a re-plot of the data from figure 9C to compare with the figure at the bottom (B). Figure 13B is the synthetic stack generated by AIMS which correlates well with the upper 33 msec of figure 13A.

Table 3.--Interval velocities derived from stacking velocities

Time (msec)	Stacking Velocity (ft/s)	Interval velocity (ft/s)
0	1,500	1,500
16	1,500	4,450
20	2,400	2,864
25	2,500	10,695
29	4,600	6,600
35	5,000	6,280
55	5,500	7,544
100	6,500	

the reflections (Dobrin, 1976). We can use these interval velocities to translate reflection times directly to depth. With this procedure the reflection times above translate to depths of 12, 21, 33, and 54 ft, respectively. Shelby-tube samples taken from boring 3 (see Table 1) confirmed soft to hard lithological contrasts (low to high velocity) at or quite near the first three of these depths. The confined water layer was encountered at 13 ft in drill hole 3 and corresponds to the horizon seen at 16 msec on the reflection record. Shelby tube 5 (ST5) cored through a sand/well-cemented sandstone layer at 19 ft and another sand/sandstone interface at 21 ft. These sandstones provide the proper lithological contrasts that generated the event on the reflection record at 20 ms. The event seen at 26 ms (equivalent calculated depth: 33 ft) on the reflection record can be tied to a pair of clay/well-cemented sandstone interfaces seen in Shelby tubes 7 and 8 (ST7 and ST8 of fig. 3) from 28.5 to 30.5 ft. The event at 31 ms (calculated depth: 54 ft) on the reflection record goes beyond the depths to which Shelby-tube core samples were taken; however, downhole seismic data did encounter a significant velocity contrast at this depth (fig. 4). Downhole and refraction data can also be used to support depths to the shallow layers calculated from reflection data. The downhole data shows strong velocity contrasts at 14, 20, 26, 30 and 33 ft all of which support the reflection data. Refraction data (see Refraction Seismic Survey discussed earlier) supports the reflection data at two of the times: 16 ms (calculated depth: 12 ft) and 20 ms (calculated depth: 21 ft). Here, refractions identified significant velocity contrasts at approximately 12 and 23 ft; though alternating low- and high-velocity layers may preclude energy returns from all layers and accurate calculation of depths to those beds. In spite of the inaccuracies involved, three separate lines of investigation seem to validate the reflection data and help to substantiate the information derived from it.

SEISMIC MODELING

AIMS was used to generate the seismic response of the geologic model (derived from downhole and refraction data). The modeling produced a reasonable match to the original seismic reflection section, giving greater confidence in the reflection data and geologic interpretation (fig. 13B). The geologic model used as input to AIMS was constructed from information collected during downhole and refraction seismic experiments (see section on Field Site Documentation). Interpretation of these data produced a model consisting of 12 flat layers (called horizons in AIMS) shown in figure 14. The horizons in AIMS are defined by horizontal extent and depth in feet and then assigned a number. The horizons mark boundaries where a strong acoustical contrast was observed in the downhole and refraction experiments. A seismic velocity determined previously is assigned to the horizon and that velocity is held constant over the entire depth of that horizon. Next, a ray, representing a point source on a seismic wavefront, is traced perpendicular to each horizon at a user-defined interval. As these rays cross the boundary between two horizons the amplitude value represented by the velocity contrast at that boundary is calculated and stored for later use. The two-way traveltime is also calculated and stored. The relative amplitudes and traveltimes to all horizons are displayed in figure 15A. Diffracted rays were not included in the ray tracing model. Convolving a synthetic source pulse, with the appropriate spectral character of the 12-gauge shotgun, produces the

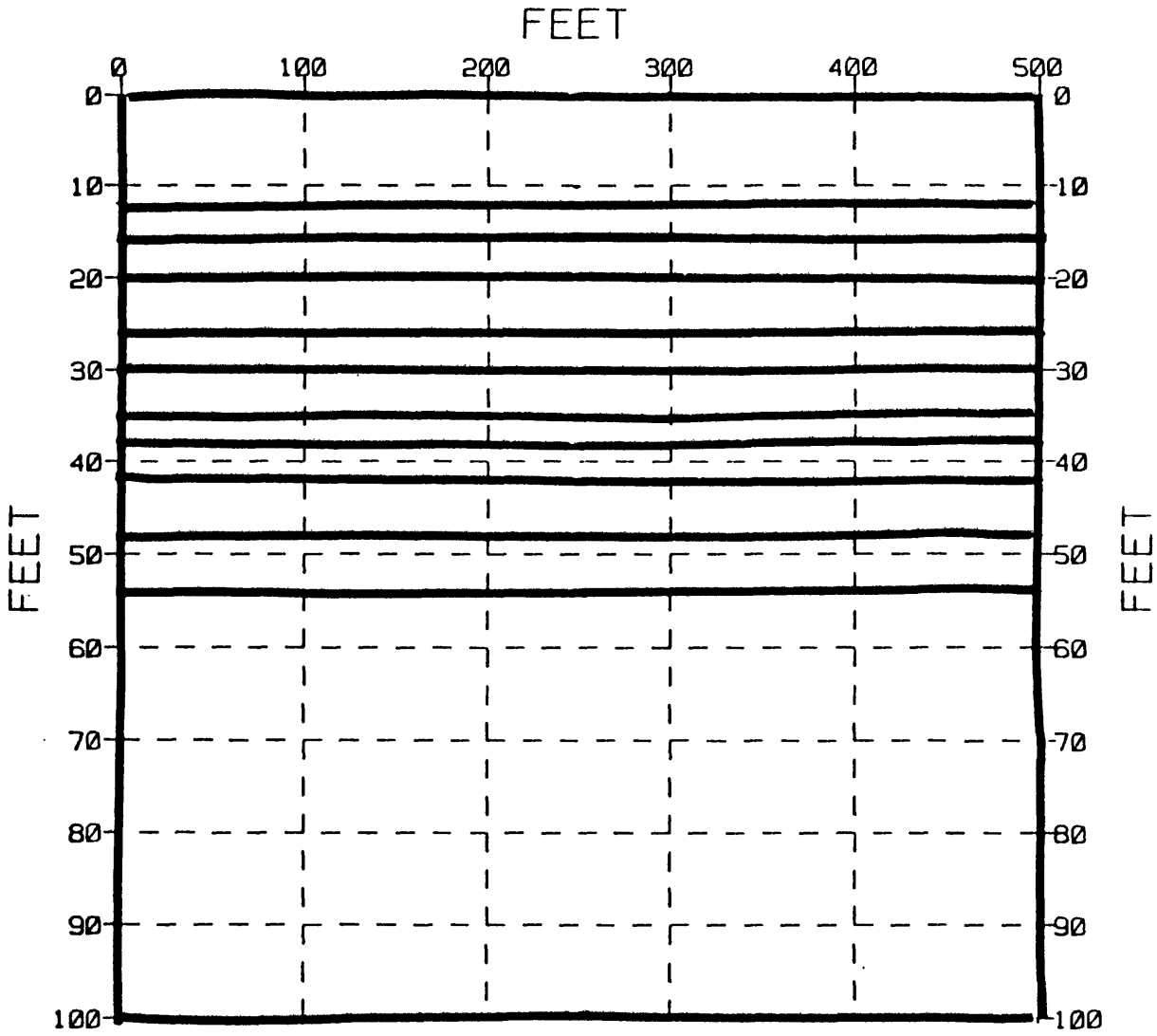

Figure 14.--This figure shows the depth model used to generate the synthetic stack section.

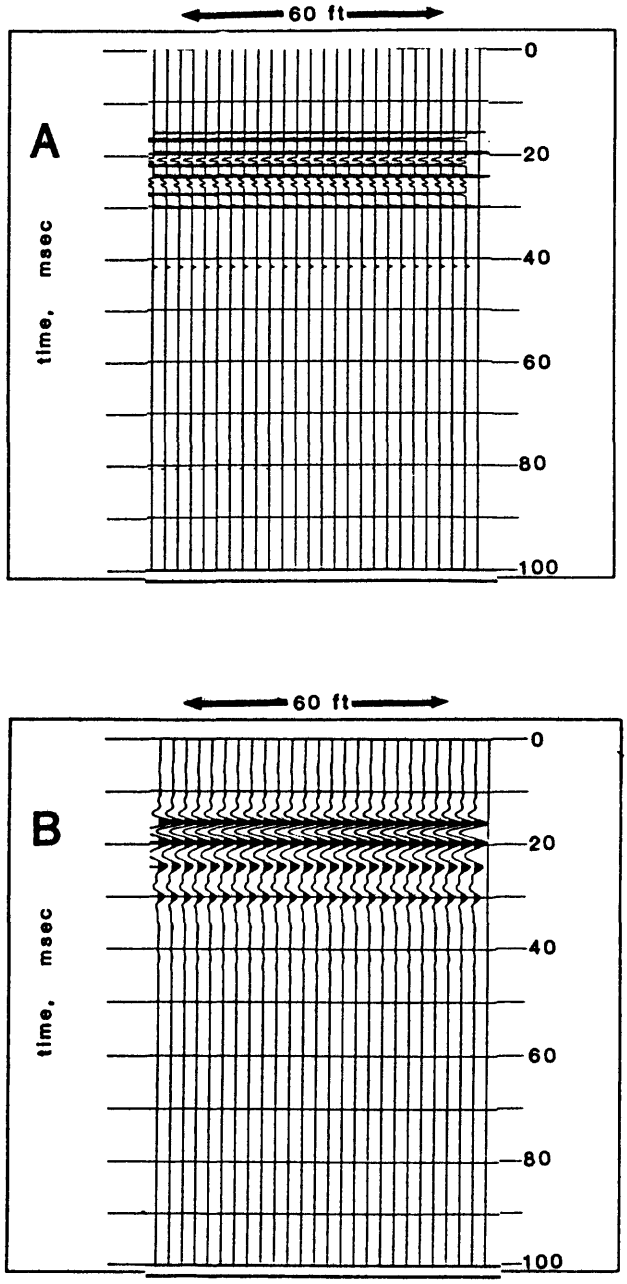

Figure 15.--The top diagram (A) shows the calculated amplitudes and traveltimes generated by the AIMS modeling for the 12 horizons seen in the depth model of figure 14. The bottom figure (B) is the result of filtering the data of 15A with an estimated seismic source wavelet.

two-dimensional seismic response of the geologic model. Spreading and transmission losses that occurred in the real world, as well as interference due to random noise, have been ignored. Figure 15B is the seismic response of a 75, 150-300, 450 Hz band-pass filter convolved with the relative amplitude spikes calculated in the previous step. Figure 15B can be considered to be an approximate stack section.

Synthetic Stack versus Real Data

Figure 16 compares the AIMS synthetic stack section to the real reflection data and reveals some strong similarities between the two. Primarily, these similarities occur among the first four coherent reflecting events found at similar times on both figures. Many horizons were not resolved due to the frequency band and source pulse length of the shotgun. The horizons which generated positive peak reflections on the synthetic section correspond to depths of 12, 20, 35, and 55 ft. Horizons with a total vertical extent of less than 3 feet and a corresponding high velocity assigned to that layer were not resolved accurately. Also, the synthetic process for stack generation used here has slightly better resolution than the real data. The reason the synthetic is better may be due either to inaccurate bandwidth characterization for the synthetic source pulse, to the need to consider diffracted rays, or noise. In summary, a strong similarity between real reflection data and seismic modeling suggests that subsurface acoustic boundaries as shallow as 12 and 20 ft produced clearly resolved reflections on the real seismic reflection data.

CONCLUSIONS

Subsurface information gathered through uphole/downhole seismic surveys, seismic refraction, borehole cores, and seismic modeling verified that the reflection equipment used in this experiment detected horizontally layered strata in the 12- to 55-ft depth range. Air-blast and ground-roll energy from the shotgun dominated much of the reflection record and posed a problem in the computer processing of this data. Future refinements (now planned or installed) to the equipment such as: use of higher frequency low-cut recording filters and a seismic source with better confinement of the air blast would help solve these problems in the field rather than in the processing center. These refinements would also improve the resolution of reflection events and extend the depth of penetration achieved in this experiment.

With the techniques learned in this experiment and the refinements in place, the seismic reflection equipment used here would be effective in examining near-surface structure in recently faulted terrains, on landslides, and perhaps in the correlation of reflection data with site response investigations.

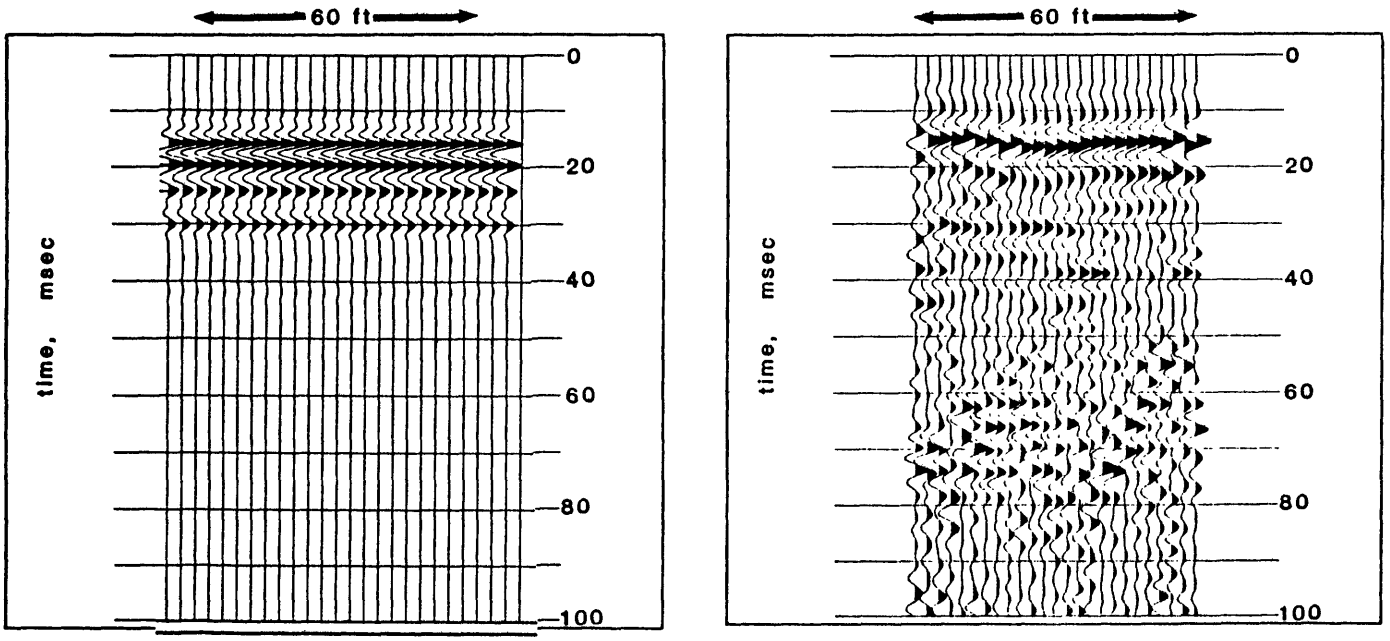

Figure 16.—The figure at left is the synthetic stack generated by AIMS to compare with the real reflection data on the right.

REFERENCES

Berkhout, A. J., 1977, Least squares inverse filtering and wavelet deconvolution: Geophysics, v. 42, no. 7, p. 1369-1383.

Dobrin, M. B., 1976, Introduction to geophysical prospecting: New York, McGraw Hill Book Co., 630 p.

Hunter, J. A., Burns, R. A., and Good, R. L., 1981, Optimum field techniques for bedrock mapping with the multichannel engineering seismograph [abs.]: Geophysics, v. 46, p. 451.

Hunter, J. A., Pullan, S. E., Burns, R. A., Gagne, R. M., and Good, R. L., 1984, Shallow seismic reflection mapping of the overburden-bedrock interface with the engineering seismograph--Some simple techniques: Geophysics, v. 49, p. 1381-1385.

Input-Output Inc., 1980, Instrument manual--DHR 2400 Digital Tape Format Manual, I/O 105349: Houston, Texas.

Jurkevics, Andrejs and Wiggins, Ralphe, 1984, A critique of seismic deconvolution methods: Geophysics, v. 49, no. 13, p. 2109-2116.

Lang, D. G., 1980, Seismic field technology: Petty-Ray Geophysical Division, Houston, Texas, p. 28-29.

Mooney, H. M., and Kaasa, R. A., 1962, Air waves in engineering seismology: Geophysical Prospecting, v. 10, no. 1, p. 85-92.

Sengbush, R. L., 1983, Seismic exploration methods: International Human Resources Development Corporation, Boston, Mass., 296 p.

Appendicies 1 and 2.--Borehole Information

Appendix 1.--Log of boring 2

Sample no.	Depth (ft)	Description
		No samples taken above 13 ft.
1	13-17 Including Shelby-tube samples ST1-4 from DFC DH no. 3	Sand, fine and silt, brown, noncalcareous, low to dense, moderate plasticity with 20-30 percent coarse sand and fine gravel and moderate amount of clay. Sand angular to subangular quartz, feldspar, biotite and ferromags. Coarse sand and gravel of quartz, feldspar, biotite, fine-grained granite, andesite and rhyolite porphyry, biotite schist, biotite gneiss. Gravel-size material of angular fragments of siltstone and sandstone.
2	17-24 Including Shelby-tube samples ST 5 and 6	Sand, medium to coarse, dark-gray-brown, non calcareous, low to very low plasticity with 10-20 percent fine sand and silt and 10 percent fine-to medium-size gravel. Small amount clay. Sand predominantly angular to subangular rock predominantly of fine-grained granite and andesite porphyry. Fine sand predominantly angular quartz, ferromags., biotite and muscovite. Gravel-size material mostly angular fragments of siltstone and sandstone with rounded granite, andesite, rhyolite and basalt porphyry. Fine sand increasing to 30 percent at basal contact.
3	24-35 Including Shelby-tube samples ST 7-9	Sand, fine to medium, dark-gray-brown, non calcareous, dense, low to very low plasticity, except low to moderate from 30-32 ft. As much as 20 percent coarse sand and small fine gravel, small amount fine gravel, clay with increase from 30-32 ft, and silt. Fine sand and silt angular and predominantly quartz, biotite, ferromags, and feldspar. Medium and coarse sand angular to subrounded, predominantly andesite, rhyolite, basalt, fine-grained granite and gneiss. Fine gravel-size material, mostly angular siltstone and sandstone with some rounded andesite, rhyolite, basalt, and fine-grained granite.

Appendix 1.--Log of boring 2--Continued

Sample No.	Depth (ft)	Description
4	35-39 Including Shelby-tube samples ST 10-11 (in part)	Clay, dark-greenish-gray, silty, sandy, gravelly, non-calcareous, moderate plasticity. Fine sand and silt mostly of angular quartz, feldspar, and ferromags. Medium and coarse sand mostly intermediate composition igneous rocks and assoc. feldspar, and little fine-grained granite. Fine gravel-size material mostly siltstone and sandstone fragments.
5	39-41 Including Shelby-tube samples ST 11 (in part), ST 12 (in part)	Sand, medium to coarse, dark-brown, non calcareous, low plasticity with abundant coarse sand to fine gravel silt of angular fragments of siltstone and sandstone. Trace of fine sand and silt and clay. Composition similar to above.
	41-44 Including ST 12 (in part), ST 13 (in part)	No recovery-assume sand.
6	44-45 Including Shelby-tube sample ST 14	Sand, medium, dark-greenish-gray, noncalcareous, low plasticity with fine sand and silt and approximately 10 percent coarse sand and fine gravel, mostly of intermediate composition igneous rocks with some rhyolite, granite and metamorphic rocks.
	45-48	No recovery-assume sand.
7	48-50	Clay, dark-greenish-gray, noncalcareous, moderate to high plasticity, with about 10 percent fine sand and silt with little medium to coarse sand and fine gravel.
	50-53	No recovery-assume sand.

Appendix 1.--Log of boring 2--Continued

Sample No.	Depth (ft)	Description
8	53-55	Sand, dark-greenish-gray, fine- to medium-grained, noncalcareous, low plasticity, with 10-20 percent coarse sand and fine gravel, latter mainly siltstone and sandstone fragments. Fine sand and silt, angular quartz and feldspar, medium to coarse sand of quartz, feldspar, acidic to medium composite igneous rocks.
	55-57	No recovery-assume sand.
9	57-60	Clay-sand mixture, dark-greenish-gray, non calcareous, moderate plasticity with silt to coarse sand and some angular fine gravel fragments of siltstone and sandstone.

Appendix 2.--Soil sample test results

Submitter: Mr. R. Johnson
Location: Denver, Colorado
Project No.: 9950-01919
Date: February 5, 1985
Analyst: A. Shanahan/L. Chandler
Reviewed by: George S. Erickson

Sample No.	Particle size distribution[1] A.S.T.M. classification: Gravel 4.76 (mm) +200	Sand 4.76-0.075 (mm)	Silt 0.075-0.005 (mm)	Clay 0.005 (mm)	Reaction with 10 percent HCL	Magnetic properties	Grain[2] density on +40 material	Grain[2] density on -40 to material
FCS 1	2	54	26	18	None	Yes	2.78	2.98
FCS 2	2	60	20	18	Moderate	Yes	2.85	2.88
FCS 3	5	61	19	15	Moderate	Yes	2.86	2.85
FCS 4	2	45	34	19	Weak	Yes	2.71	2.86
FCS 5	7	48	26	19	Weak	Yes	2.69	2.71
FCS 6	3	42	27	28	None	Yes	2.73	2.83
FCS 7	2	23	26	49	None	Yes	2.74	2.77
FCS 8	1	42	35	22	None	Yes	2.84	2.75
FCS 9	1	44	33	22	None	Yes	2.73	2.79

[1]Percent of dry soil weight
[2]gm/cc.